Applied Catalysis B: Environmental 180 (2016) 707–714

Contents lists available at ScienceDirect

Applied Catalysis B: Environmental

journal homepage: www.elsevier.com/locate/apcatb

Role of Fe/pumice composition and structure in promoting ozonation reactions

Lei Yuan[a,c,*], Jimin Shen[b], Zhonglin Chen[b,**], Xiaohong Guan[a]

[a] State Key Laboratory of Pollution Control and Resources Reuse, College of Environmental Science and Engineering, Tongji University, Shanghai 200092, PR China

[b] State Key Laboratory of Urban Water Resource and Environment, School of Municipal and Environmental Engineering, Harbin Institute of Technology, Harbin 150090, PR China

[c] National and Provincial Joint Engineering Laboratory of Wetland Ecological Conservation, Heilongjiang Academy of Science, Harbin 150040, PR China

ARTICLE INFO

Article history:
Received 12 May 2015
Received in revised form 5 July 2015
Accepted 11 July 2015
Available online 21 July 2015

Keywords:
Ozone
Ozone adsorption
Fe modified pumice
Hydroxyl radical
Enhancement mechanism

ABSTRACT

The catalytic effectiveness and mechanism of Fe/pumice in heterogeneous catalytic ozonation of *p*-chloronitrobenzene (*p*-CNB) is investigated in batch mode. The results indicate that Fe/pumice significantly increased the removal efficiency of *p*-CNB, the utilization efficiency of ozone, and the production of hydroxyl radical (•OH) relative to pumice during catalytic ozonation. The mesopority of the Fe/pumice surface is a key factor due to its ozone adsorption ability. The surface hydroxyl groups on Fe/pumice metal oxides are ozone decomposition sites. The dominant oxide species in the ozonation reaction process is •OH. The zero-charged surfaces of the Fe/pumice was favorable for catalytic ozonation. The results of the investigation of the enhancement mechanism confirm that Fe-modified pumice increases the number of surface hydroxyl groups and the degree of ozone adsorption on the catalyst surface, resulting in enhanced collision probability between surface hydroxyl groups on Fe/pumice metal oxides and ozone molecules to accelerate •OH from ozone decomposition and to promote *p*-CNB removal from aqueous solution.

1. Introduction

The effective removal of organic pollutants is a primary objective of drinking water and wastewater treatment industries. Sole ozonation is a suitable technical option in the removal of organic pollutants. Numerous organic pollutants are easily degraded by ozone molecules, but many emerging contaminants are refractory to ozone. Thus, the effective removal of refractory organic pollutants by sole ozonation is challenging. Modifications of ozonation technology, such as heterogeneous/homogeneous catalytic ozonation, H_2O_2/O_3, UV/ H_2O_2/O_3, and UV/O_3, is required to increase the oxidizing capability and removal effectiveness of sole ozonation [1]. The most significant characteristic of the above technologies is the generation of •OH, which is the primary secondary oxidant species that comes from dissolved ozone decomposition.

As a modified ozonation process, heterogeneous catalytic ozonation is of interest to drinking water and wastewater treatment industries for its potentially significant effectiveness and minimal detrimental effect on water quality [2]. In recent years, heterogeneous catalytic ozonation studies mainly focused on increasing ozone mass transfer and amount of •OH generation. Heterogeneous catalysts commonly used for this process include activated carbon [3–5], metal oxides [2,6–12], and metals on supports [13–19]. However, industrial-scale application of these materials is inhibited by their complex separation, low mechanical strength, high cost, or easy oxidation.

Natural pumice was used as an ozonation catalyst in our previous study, where it showed promising catalytic activity [20]. Pumice, which is a composite silicate material from volcanic eruption, is widely used in adsorbent [21,22] and photocatalyst [23,24] preparation in drinking water and wastewater treatment. Pumice was selected as a support because of its high mechanical strength, stability, separation ability, and catalytic effectiveness.

At present, α-FeOOH received significant attention in catalytic ozonation [25]. Synthetic α-FeOOH exhibits higher catalytic ability than widely used metal oxide catalysts such as Fe_2O_3, MnO_2, CuO, NiO, and Co_3O_4 [26]. However, separation difficulty impairs the use of α-FeOOH in drinking water and wastewater treatment

* Corresponding author at: State Key Laboratory of Pollution Control and Resources Reuse, College of Environmental Science and Engineering, Tongji University, Shanghai 200092, PR China.
** Corresponding author. Fax: +86 451 86283028.
E-mail addresses: yuanleihit@163.com (L. Yuan), zhonglinchen@hit.edu.cn (Z. Chen).

http://dx.doi.org/10.1016/j.apcatb.2015.07.016
0926-3373/

industries. To enhance the catalytic capacity of pumice and the ease of use of α-FeOOH, pumice-supported α-FeOOH (Fe/pumice) was used as an ozonation catalyst for the removal of organic pollutants in water.

The compound *p*-chloronitrobenzene (*p*-CNB) is a typical halogenated nitro-aromatic compound extensively used in many fields and detected in natural water [27]. The considerably low reactivity of *p*-CNB towards biodegradation makes it harmful to aquatic environments. In addition, *p*-CNB is difficult to remove using chemical oxidation and has low adsorption onto solid surfaces [20,27–29]. Therefore, *p*-CNB was a well suited model pollutant for catalytic ozonation testing.

This study investigated (1) the effectiveness of Fe/pumice in catalytic ozonation; (2) oxidant species and active sites; (3) ozone mass transformation and conversion on heterogeneous surfaces; and (4) the enhancement mechanism.

2. Methodology

2.1. Materials and reagents

Natural pumice powder composed of 0.3–0.5 mm particles was obtained from China Zhangjiakou. Compounds *p*-CNB (purity ≥ 99.5%) and 5,5-dimethyl-1-pyrroline-*N*-oxide (DMPO, purity ≥ 98%) were purchased from Chem Service. Ultrapure water (≥18 MΩ cm) used throughout this study was obtained from a Milli-Q Water System. Other chemicals such as $Fe(NO_3)_3$, HCl, NaOH, and $Na_2S_2O_3$ were of analytical grade and were used as received.

Fe/pumice catalyst was prepared using the methods described by Yuan et al. [29]. Pumice powders completely absorbed $Fe(NO_3)_3$ as a precursor substance, which were impregnated with NaOH for 12 h. The catalyst was collected and washed with distilled water until the pH of rinse distilled water remained constant. The catalyst was dried at 60 °C for 12 h using an air dry oven and was kept in a desiccator before use.

2.2. Experimental procedure

Ozonation tests were conducted in batch mode. The ozonation reactor was a modification flask with an effective solution volume of 1.0 L. Ozone was generated through an ozonizer (COM-AD-01, Germany) with dry oxygen as the supply gas. Low flow ozone was bubbled in the ultrapure water (1 L) in the reactor to achieve the desired concentration. The catalyst powder and the *p*-CNB stock solution were then immediately added to the stock ozone solution. A magnetic stirrer continuously mixed the solution. Samples collected from the reactor at different time intervals (0, 2, 4, 6, 10, and 15 min) were immediately quenched into an excess of $Na_2S_2O_3$ solution to remove residual ozone. The quenched samples went through filters (0.45 μm) prior to determination of residual *p*-CNB.

The amount of ozone adsorption on catalyst experiments was determined using the reaction system above with the same reaction conditions. The catalyst was immediately added to the stock ozone solution. Samples were taken at different time intervals and then mixed with indigo solution according to the indigo method. The mixture solution was kept for 12 h. The concentration of dissolved ozone (before and after 12 h) was determined.

2.3. Analytical method

The chemical composition of catalysts was detected with an X-ray fluorescence (XRF) spectroscopy system (AXIOS-PW 4400, Netherlands). The crystalline structure of the catalysts was detected with an X-ray diffraction (XRD) analyzer (D8 Advance diffractometer, Germany). Infrared spectra of catalysts were analyzed using a Fourier transform infrared (FT-IR) spectrum instrument (Spectrum One, USA). The structure of catalysts was detected based on the Brunauer–Emmet–Teller (BET) method using an accelerated surface area and porosimetry instrument (ASAP 2020, USA). The amount of •OH generated in the reaction system was captured via EMX-8/2.7 ESR (Germany).

Residual *p*-CNB was analyzed via LC-1200 (USA) with an Agilent C18 (150 mm × 4.6 mm) column using UV detection at a wavelength of 265 nm. The mobile phase was composed of 80% water and 20% methanol. The dissolved ozone concentration was analyzed via the indigo method [30]. The surface hydroxyl groups of catalysts were analyzed via the saturated deprotonation method [31]. The point of zero charge (pH_{PZC}) of catalysts were analyzed via acid–base titration method [32]. An inductively coupled plasma emission spectrometer (Optima 5300DV, USA) was used to determine the ions concentration in the aqueous solution.

3. Results and discussion

3.1. Characterization

The pumice and Fe/pumice catalysts were characterized using XRF, XRD, FT-IR, and BET techniques to determine the relationship between the microstructure of the catalysts and their catalytic ozonation activities.

The results of the XRF analysis reveal that pumice was composed of O (44.1%), Si (24.8%), Al (9.2%), Fe (7.7%), Ca (5.2%), Na (3.5%), Mg (1.5%), and K (1.8%), and the Fe/pumice catalyst was composed of O (45.8%), Si (20.5%), Fe (13.8%), Al (7.6%), Ca (4.5%), Na (3.0%), Mg (1.3%), and K (1.6%).

XRD patterns of pumice and Fe/pumice catalysts are shown in Fig. 1A. Result analysis identifies that the major phases of pumice samples were albite, anorthite, and hematite. The Fe/pumice catalyst showed different XRD patterns than the pumice supports. The loading of Fe resulted in the growth of new crystalline α-FeOOH.

In FT-IR spectra, surface hydroxyl group peaks in the stretching mode range from 3200 to 3650 cm^{-1} [33]. Fig. 1B shows that the surface structure hydroxyl group on pumice peaked at 3626 cm^{-1}, which represents Ca—OH, Na—OH, Mg—OH, or K—OH. The surface hydroxyl group on Fe/pumice peaked at 3416 cm^{-1}. Introduction of α-FeOOH significantly increased the height and width of surface hydroxyl group peaks. Thus, the surface hydroxyl group peak of Fe/pumice denotes a mixture of water peak in stretching mode at 3390 cm^{-1} (bending mode at 1620 cm^{-1}) and a surface structure hydroxyl group of α-FeOOH peaks at 3145 cm^{-1} [34]. Furthermore, the peaks at 1120 and 1008 cm^{-1} represent the Si—O—Si and Si—O—Al bonds in the stretching mode. The peaks at 800 and 638 cm^{-1} represent the bending vibration of Fe—OH and stretching vibration Fe—O bonds [35].

The physisorption isotherms of pumice and Fe/pumice catalysts are shown in Fig. 1(C). The reversible isotherm of pumice was a typical type II, indicating the presence of macroporous materials. Fe/pumice catalysts exhibited the type IV isotherm of mesoporous materials with a hysteretic loop in the range from 0.4 to 1.0 P/P_0. The pore size distribution in Fig. 1(D) was calculated according to the Barrett–Joyner–Halenda method. The results show that Fe/pumice exhibits a significantly narrower mesoporous pore size distribution, where pores range from 2.7 to 7.3 nm. The BET surface area converts from 0.12 m^2/g of pumice to 33.5 m^2/g of Fe/pumice, namely more than 279 times higher than specific surface area of pure pumice. The loading of α-FeOOH slight increase the pH_{PZC} from 6.12 of pumice to 6.37 of Fe/pumice. Furthermore, the quantification results show that the concentration of surface hydroxyl groups increases from 0.33 mmol/g of pure pumice to

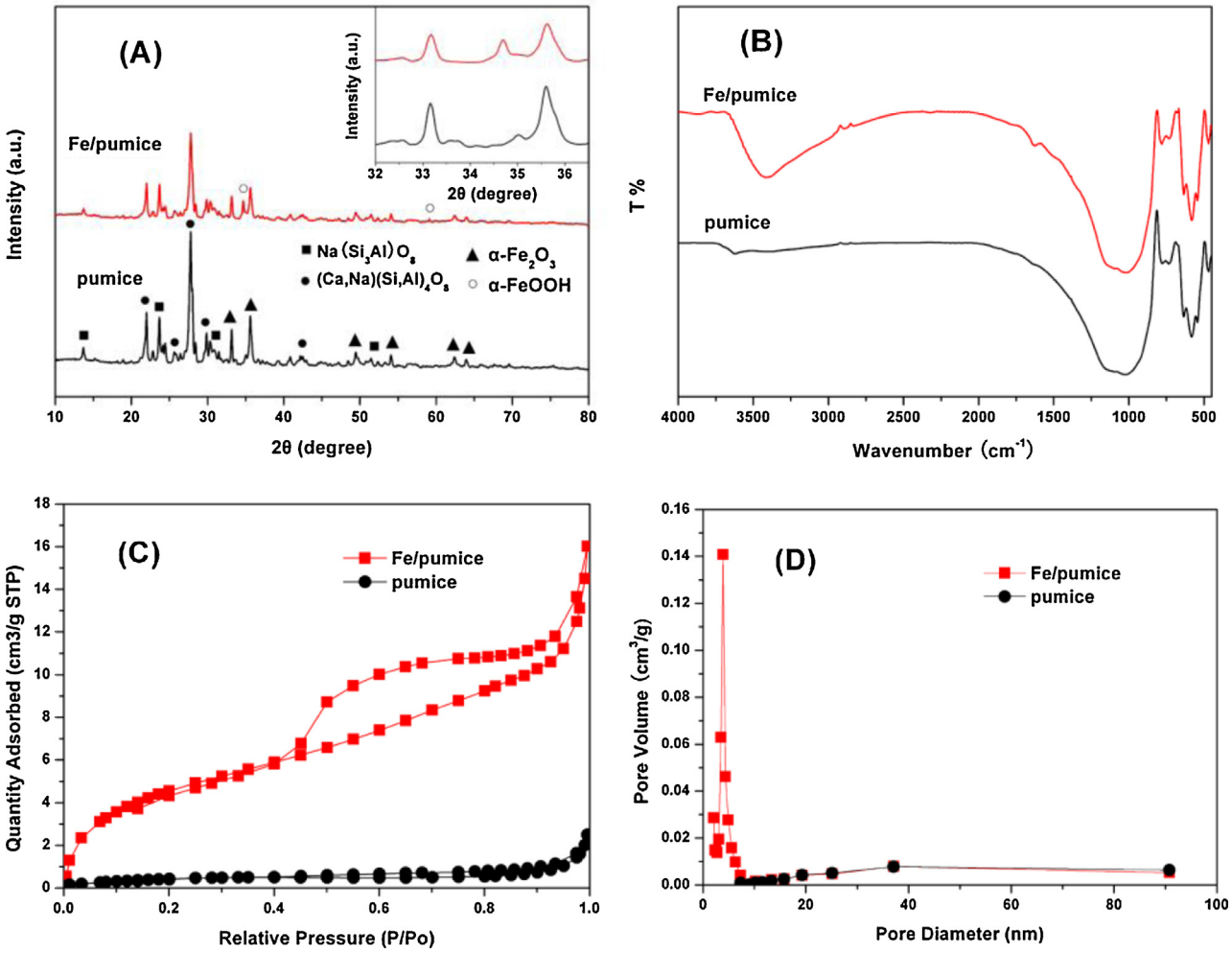

Fig. 1. Characterization of pumice and Fe/pumice catalysts: (A) XRD patterns, (B) FT-IR spectra, (C) Physisorption isotherms, (D) Pore size distribution.

Table 1
Refined physicochemical parameters of catalysts

Samples	Loading percentage of Fe (wt.%)	BET surface area (m^2/g)	Average pore diameter (nm)	SiO_2/metal oxide mass ratio	pH_{PZC}	Surface hydroxyl (mmol/g)
Pumice	–	0.12	121.5	1.09	6.12	0.33
Fe/pumice	6.1	33.5	3.2	0.84	6.37	0.58

0.58 mmol/g of Fe/pumice. The data were investigated and summarized in Table 1.

3.2. Catalytic effectiveness

The catalytic activity of Fe/pumice was evaluated via the removal efficiency of *p*-CNB in different reaction systems, including adsorption, sole ozonation, and catalytic ozonation processes. Pumice was selected as the reference in this study. The plot of *p*-CNB removal efficiency vs. reaction time was shown in Fig. 2.

Results presented in Fig. 2 indicate that *p*-CNB shows minimal adsorption on pumice and Fe/pumice surfaces of less than 5.5% under current experimental conditions. Thus, adsorption removal has a slight effect on removal efficiency of *p*-CNB in catalytic ozonation process. The removal efficiency of *p*-CNB was only 40.8% after 15 min in sole ozonation. The effective removal of *p*-CNB using the sole ozonation method was difficult due to this short reaction time. The results shown in Fig. 2 also indicate that the introduction of a heterogeneous catalytic surface leads to a synergistic role with ozone molecules in *p*-CNB removal. Relative to sole ozonation, the removal efficiency of *p*-CNB in catalytic ozonation increased with pumice and Fe/pumice, and the best result was observed using Fe/pumice. The removal efficiency of *p*-CNB with Fe/pumice after 15 min was 90.8%, which is 1.2 times higher than that with pure pumice. In addition, the stability of Fe/pumice was investigated by reusing one sample of catalyst in five successive ozonation tests. In last cycle, 90.3% of *p*-CNB removal and 2.1 μg/L of iron ion leaching at catalyst concentration of 0.5 g/L were observed in the treated water. In present study, the effect of homogeneous catalytic ozonation by iron ion is insignificant relative to sole ozonation and can therefore be neglected. The concentration of other residual ions was under the detection limit. These results indicated that Fe/pumice is stable in catalytic ozonation.

In this study, α-FeOOH was used to modify pumice. After modification, the chemical composition and structure of pumice varied, resulting in enhancement of catalytic activity. Therefore, in subsequent studies, we refer to a previous study and investigate the role of Fe/pumice surface composition and structure in catalytic ozonation.

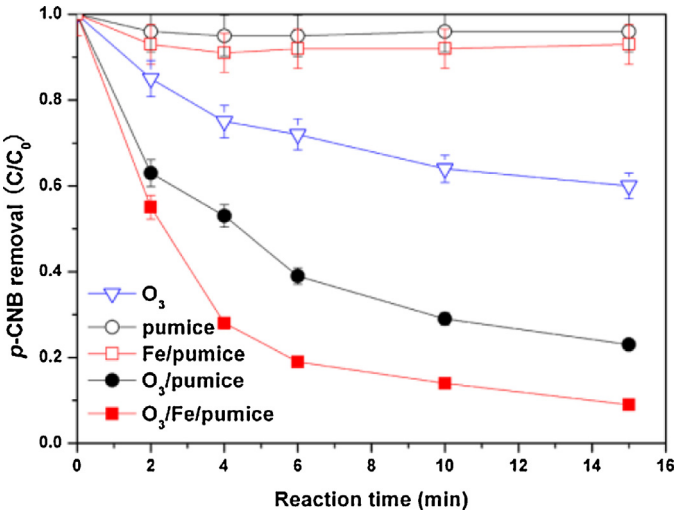

Fig. 2. Removal efficiency of *p*-CNB (initial conditions: temperature, 25 °C; pH 6.0; *p*-CNB concentration, 100 μg/L; ozone concentration, 0.9 mg/L; catalyst concentration, 0.5 g/L).

3.3. Ozone utilization efficiency

The ozone decay investigated during ozonation and catalytic ozonation exhibited different patterns of *p*-CNB removal efficiency (Fig. 3A). The presence of pumice or Fe/pumice significantly enhanced ozone decay relative to sole ozonation. However, ozonation/pumice has greater ozone decay than ozonation/Fe/pumice. A comparison between Fig. 3A and Fig. 2 shows that futile ozone consumed in pumice-catalyzed ozonation slowed down *p*-CNB removal in aqueous solution. The evaluated utilization efficiency of ozone is a primary factor in catalyst performance. Based on the data above, the utilization efficiency of ozone was expressed as follows:

$$R_U(\%) = \frac{[p-\mathrm{CNB}]_0 - [p-\mathrm{CNB}]_t}{[\mathrm{O_3}]_0 - [\mathrm{O_3}]_t} \times 100\% \quad (1)$$

where R_U is the utilization efficiency of ozone (%), subscript (0) is the initial concentration, and subscript (t) is the terminal concentration. Based on Eq. (1), a higher value of R_U represents higher ozone utilization efficiency. The results shown in Fig. 3B shows that the lowest utilization efficiency of ozone was 7.5% in sole ozonation. The R_U value for pumice-catalyzed ozonation was less than that for Fe/pumice. The R_U value for ozonation/Fe/pumice after 15 min was 12.8%, which was 1.3 times higher than that for ozonation/pumice.

In this study, the dissolved ozone in suspension may be consumed through three pathways: direct reaction of ozone molecules with *p*-CNB; decomposition of ozone molecules to active species; and absorption of ozone molecules on the catalyst surface. The rate constants of *p*-CNB with •OH and ozone are $2.6 \times 10^9\ M^{-1}\ s^{-1}$ and $1.6\ M^{-1}\ s^{-1}$, respectively, suggesting that *p*-CNB barely reacts with ozone molecule [36]. Therefore, based on the results shown in Fig. 2, the observed enhancement of R_U in the catalytic ozonation is apparently caused by higher •OH generation in the solution, especially in the Fe/pumice-catalyzed ozonation process.

3.4. Production of •OH

The oxidation of organic pollutants by dissolved ozone usually involves two routes [37]: the direct route, which involves ozone molecule oxidation, and the indirect route, which involves free radical oxidation. Dissolved ozone is unstable because of its highly active resonance structures. Ozone decomposition usually generate many intermediate species such as •OH, •O, HO_2•, HO_4•, and O^{2}• in aqueous solution. Among these, •OH is the most important free radical because of its strong oxidative capacity and unselective reaction with pollutants present in water [38]. Therefore, many studies of heterogeneous catalytic ozonation processes focus on promoting ozone decomposition to generate •OH.

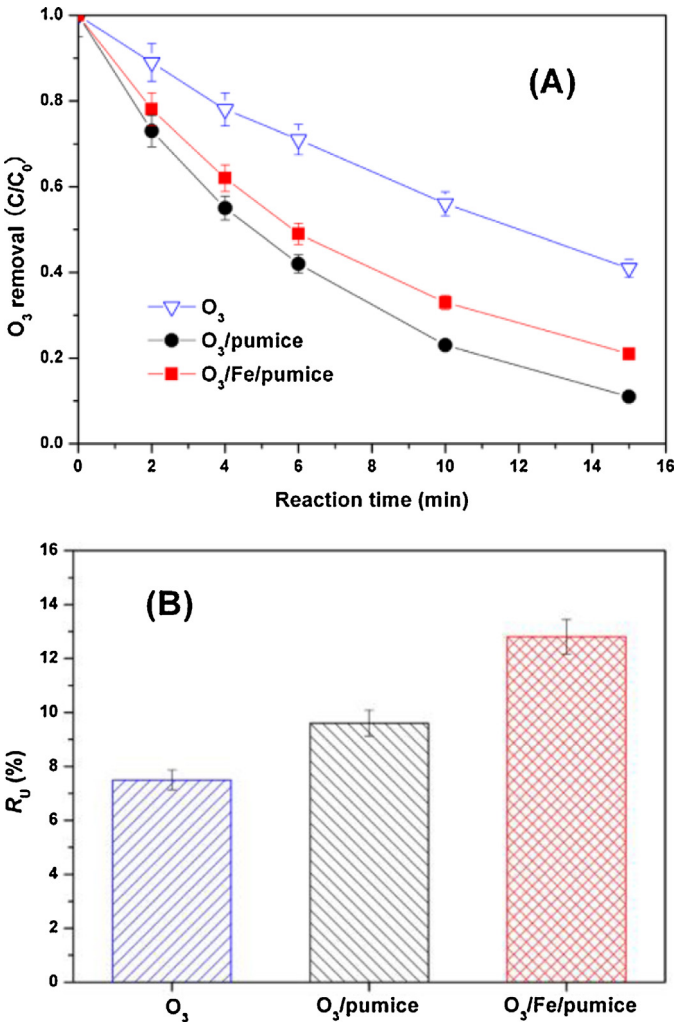

Fig. 3. (A) Ozone decay and (B) ozone utilization efficiency (initial conditions: temperature, 25 °C; pH 6.0; *p*-CNB concentration, 100 μg/L; ozone concentration, 0.9 mg/L; catalyst concentration, 0.5 g/L; (B), reaction time 15 min).

The quantification of •OH is difficult in ozonation systems because of its instability and low rate of production. The ESR spin-trap technique, which can determine •OH according to the intensity of the DMPO-OH signal, has been recently used to investigate •OH production in ozonation systems. The spectra of the DMPO-OH signal typically have four lines with a peak height ratio of 1:2:2:1. The intensity of the adduct signal increased, indicating an increased amount of •OH in the oxidized system. The tests were conducted to detect •OH generation in the sole ozonation and catalytic ozonation processes using the ESR spin-trap technique. Test results in Fig. 4 indicate that •OH generation occurs in sole ozonation and catalytic ozonation processes. The presence of pumice and Fe/pumice catalysts clearly enhanced the relative adduct signal intensity compared to that from sole ozonation. The results shown in Fig. 4 also suggest that Fe/pumice promotes ozone decomposition to generate higher amounts of •OH relative to pumice. The diversity is mainly caused by the differing surface properties of the pumice and Fe/pumice catalysts. Additionally, according to Fig. 4 and Fig. 2, a good positive correlation exists between the adduct signal intensity and the removal efficiency of *p*-CNB in the present experiment. The

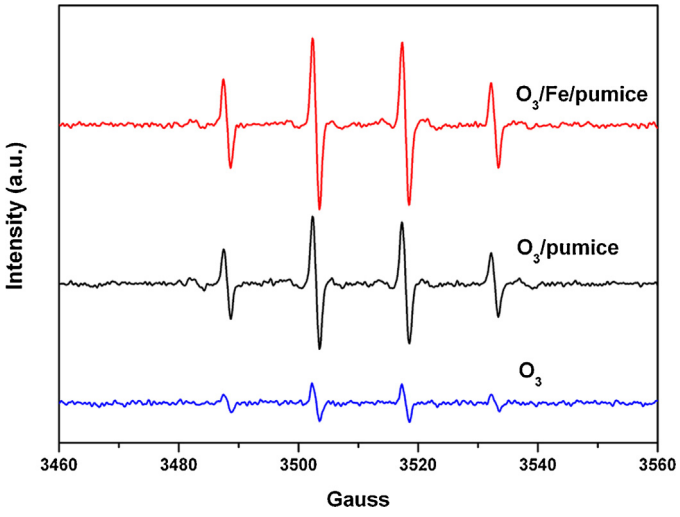

Fig. 4. Variations in intensity of DMPO-OH signal (initial conditions: temperature, 25 °C; pH 6.0; *p*-CNB concentration, 100 μg/L; ozone concentration, 0.9 mg/L; catalyst concentration, 0.5 g/L; DMPO concentration, 100 mmol/L).

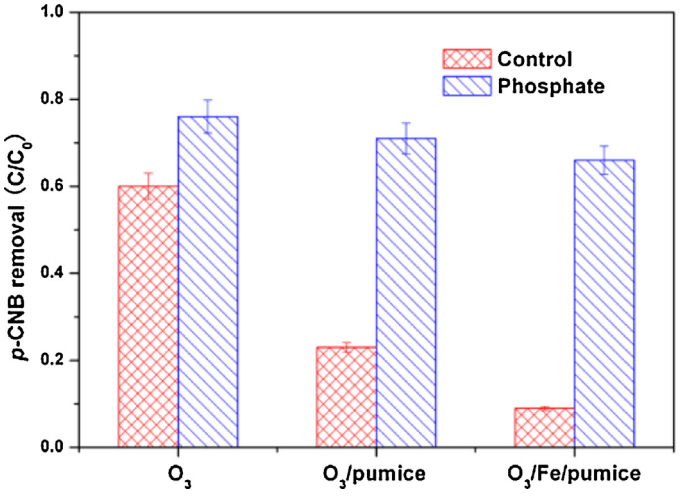

Fig. 5. Influence of phosphate on *p*-CNB removal (initial conditions: temperature, 25 °C; pH 6.0; *p*-CNB concentration, 100 μg/L; ozone concentration, 0.9 mg/L; catalyst concentration, 0.5 g/L; phosphate, 10 mmol/L; reaction time 15 min).

results also confirm that the removal of *p*-CNB in this study should be mainly attributed to •OH oxidation.

3.5. Ozone decomposition sites

Hydroxyl groups are formed on Lewis acid sites of metal oxide surfaces in the presence of aqueous solution, which function as a Brønsted acid that promotes ozone decomposition to generate •OH [39,40]. Phosphate is a Lewis base that can substitute for surface hydroxyl groups on metal oxides in aqueous suspension [41–43]. Furthermore, phosphate is also a scavenger of •OH [44]

Results shown in Fig. 5 indicate that the removal efficiency of *p*-CNB was significantly reduced with introduction of phosphate for all processes, especially in catalytic ozonation. The removal efficiency of *p*-CNB decreased in sole ozonation because of competition between phosphate and *p*-CNB for •OH consumption. In the presence of phosphate, the increment in *p*-CNB removal decreased by 48.1% for ozonation/pumice and 57.2% for ozonation/Fe/pumice, which is similar to the catalytic activity of the catalysts for ozone

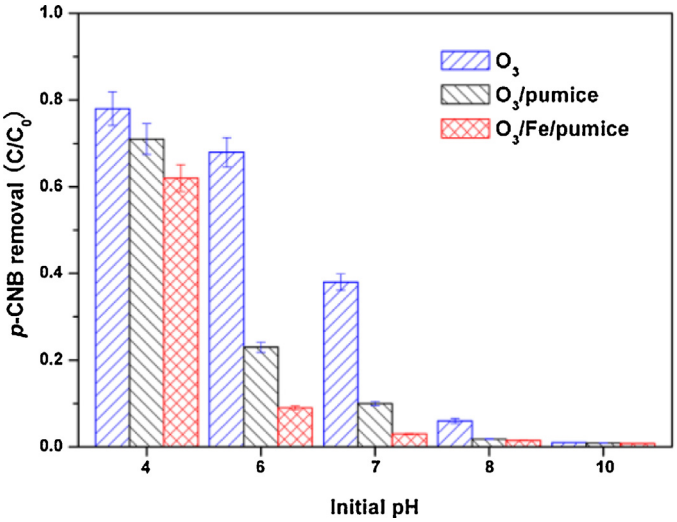

Fig. 6. Influence of initial pH on *p*-CNB removal (initial conditions: temperature, 25 °C; *p*-CNB concentration, 100 μg/L; ozone concentration, 0.9 mg/L; catalyst concentration, 0.5 g/L; reaction time 15 min).

decomposition to produce •OH, indicating that Fe/pumice has more activity for ozone decomposition to •OH than pumice. The results further indicate that surface hydroxyl groups on metal oxides of pumice and Fe/pumice are important in promoting •OH formation from ozone decomposition in catalytic ozonation, leading to a higher amount of •OH compared with sole ozonation, resulting in increased *p*-CNB removal. The results also justified that SiO_2 on pumice or Fe/pumice surfaces cannot promote the decomposition of ozone into •OH.

Sui et al. [41] reported that α-FeOOH can significantly increase the production of •OH at pH ≤ 7, resulting in conversion of organic pollutants in catalytic ozonation. Surface hydroxyl groups on α-FeOOH can also act as ozone decomposition sites to produce •OH. Table 1 and Fig. 1B show that after introduction of α-FeOOH, concentrations of surface hydroxyl groups on pumice increased, resulting in the enhancement of catalytic ability.

3.6. Effect of pH

The pH of the solution has a remarkable effect on ozone decomposition to generate •OH [45]. As shown in Fig. 6, the high solution pH enhanced the removal efficiency of *p*-CNB in sole ozonation and catalytic ozonation. Meanwhile, Fe/pumice exhibited high catalytic activity in solution pH levels ranging from 4 to 10, particularly at solution pH 6 and 7. When solution pH either decreased to 4 or increased to 10, the catalytic activity of Fe/pumice was inhibited. The surface hydroxyl groups of catalyst exhibit pH-dependent charge in solution [39]. The zero-charging of pumice surface (a solution pH close to pH_{PZC}) in water benefited ozone decomposition for •OH generation [20], consistent with the results found in Fe/pumice-catalyzed ozonation of *p*-CNB.

3.7. Amount of ozone adsorption

The ozone gas–liquid mass transfer from aqueous solution to catalyst surface has a significant role in catalytic ozonation effectiveness. Therefore, the ozone adsorption properties of pumice and Fe/pumice were investigated (Fig. 7).

As shown in Fig. 7A, the ozone removal increased with reaction time in ozone decomposition and catalytic ozone decomposition. The concentration of dissolved ozone also decreased in sole ozone because of self-decomposition. The ozone decay rate

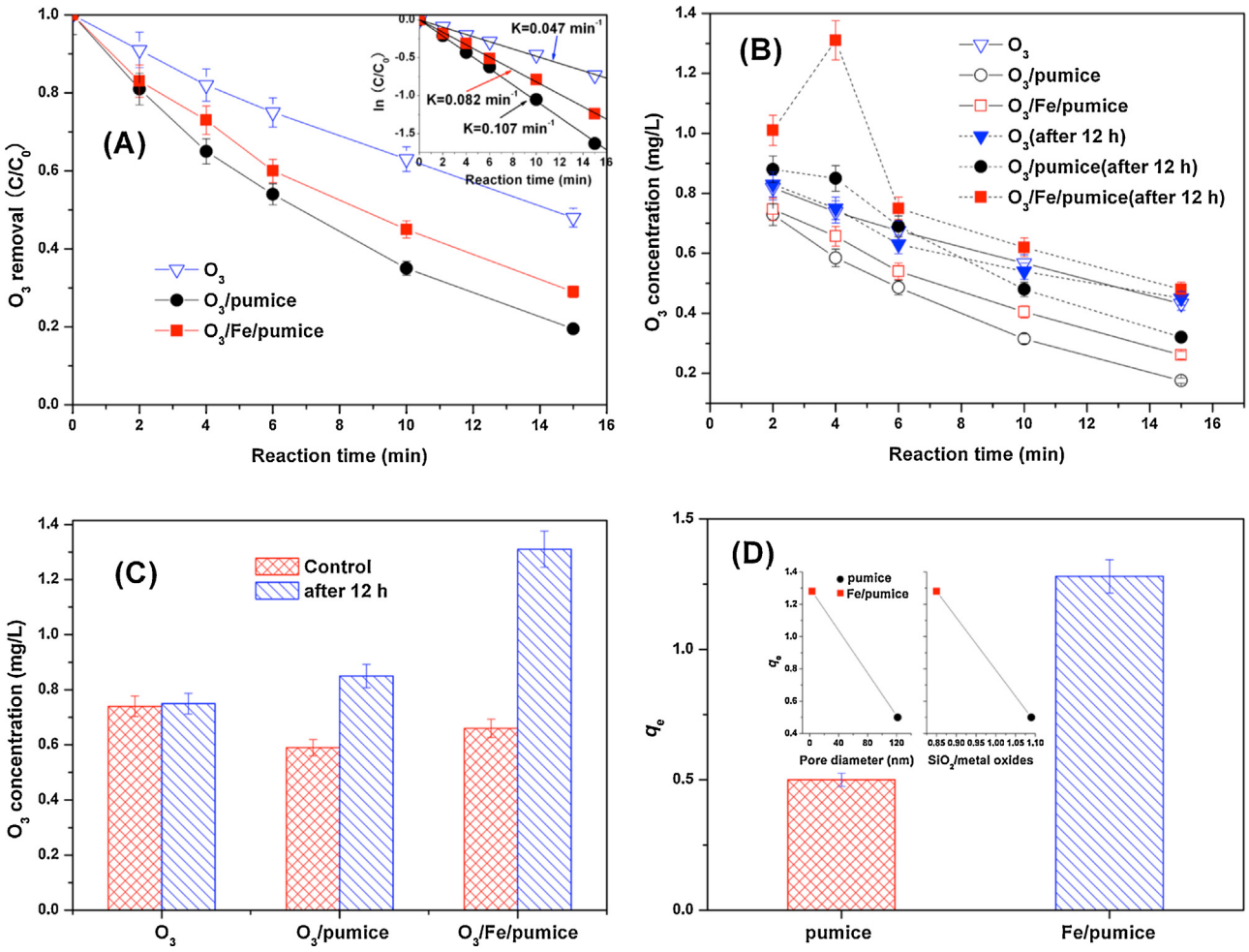

Fig. 7. (A) The catalytic ozone decomposition, (B) the ozone concentration before and after 12 h, (C) the ozone desorption concentration, and the ozone adsorption amount (initial conditions: temperature, 25 °C; pH 6.0; ozone concentration, 0.9 mg/L; catalyst concentration, 0.5 g/L).

increased relative to sole ozone with the introduction of pumice and Fe/pumice catalysts. The inset of Fig. 7A shows ozone decay compared with a first-order kinetics model. The first-order rate constant significantly increased with the introduction of pumice and Fe/pumice, with the first-order rate constant increasing 2.28- and 1.74-fold, respectively. Comparing Fig. 7A with Fig. 4, it can be observed that pumice enhanced the rate of ozone decay to •OH relative to Fe/pumice.

The concentration of dissolved ozone (before and after 12 h) in the sole ozone and catalytic ozone processes with specific time intervals was determined according to the indigo method. As shown in Fig. 7B, ozone adsorption on pumice and Fe/pumice surfaces slowly occurs because of desorption in aqueous solution. After 12 h, the concentration of dissolved ozone significantly increased in the catalytic ozone decomposition system. The concentration of dissolved ozone in Fe/pumice suspension is higher than that in pumice suspension for all time intervals, especially at 4 min.

To determine the adsorption ability of pumice and Fe/pumice catalysts, a reaction time of 4 min was deemed as the optimal time interval. Fig. 7C shows that the concentrations of ozone in pumice suspension and Fe/pumice suspension significantly increased after 12 h. The Fe/pumice suspension had the highest concentration of dissolved ozone after 12 h, followed by pumice suspension and the sole ozone decomposition system. The concentrations of ozone in the ozone decomposition system slightly increased because of indigo self-decomposition. The adsorption of indigo on the catalyst surface is very low and can therefore be neglected. The increment of ozone concentration in suspension before and after 12 h represents the ozone adsorption capacity of the catalysts. The amount of ozone adsorption on the catalyst surface can be expressed as follows:

$$q_e(\mathrm{mg/g}) = \frac{(C_t - C_0)V}{M} \quad (2),$$

where q_e is the amount adsorbed, C_0 is the aqueous ozone concentration at 4 min, C_t is the aqueous ozone concentration remaining in solution after 12 h, M is the catalyst mass, and V is the volume of the solution.

The amount of ozone adsorption on pumice and Fe/pumice are 0.5 and 1.28 mg/g, respectively, according to Eq. (2) (Fig. 7D). Fujita et al. [46] reported that ozone adsorption capacity is strongly dependent on the amount of SiO_2 and the pore structure of the catalyst surface. The increased SiO_2 ratio is beneficial to the adsorption of ozone in aqueous solutions, and the adsorbed ozone was desorbed almost reversibly. However, Fig. 7D inset shows that the low SiO_2/metal oxide mass ratio and mesoporous structure of Fe/pumice was positively affected by its ozone adsorption capacity in the present experiment, indicating that ozone adsorption capacity may be dominated by pore structure on the Fe/pumice catalyst surface.

3.8. Enhancement mechanism

Based on the results obtained and the theory mentioned above, the role of the Fe/pumice surface in catalytic ozonation is proposed and illustrated in this section.

Heterogeneous catalytic ozonation as a complex oxidation system mainly involves three mechanisms [47]: (1) ozone adsorbed on the catalytic surface results in the generation of oxide species that react with organic pollutants, (2) organic pollutants adsorbed on the catalytic surface and oxidized by ozone, and (3) adsorption of ozone and organic pollutants at the same time before interacting with each other.

At first, the introduction of pumice appreciably enhances the removal efficiency of *p*-CNB relative to that in sole ozonation (Fig. 2) because the presence of the catalytic surface promotes the production of •OH. The introduction of Fe further enhances the catalytic ozonation activity of the pumice. The amount of *p*-CNB adsorbed on the pumice and Fe/pumice surfaces is insignificant. Therefore, catalytic ozonation in this experiment is dominated by the first mechanism mentioned above.

On the one hand, pumice is introduced into the aqueous solution, and water molecules are adsorbed onto the pumice surface. The adsorbed water then dissociates into the hydroxyl ion and hydronium, which form surface hydroxyl groups. Modification by increasing Fe results in the enhancement of surface hydroxyl groups (Table 1). The results in Fig. 5 show that surface hydroxyl groups on metal oxides of pumice and Fe/pumice are ozone decomposition sites in catalytic ozonation. On the other hand, the results in Fig. 7 indicate that pumice and Fe/pumice catalysts can adsorb ozone in aqueous solution. Fe-modified pumice exhibits mesoporous structure on Fe/pumice catalysts, which results in the enhancement of the amount of ozone adsorption.

A comparison between Fig. 7 and Fig. 2 revealed that a high amount of ozone adsorption at 4 min corresponds to a high rate of *p*-CNB removal in aqueous solution, indicating the enhancement of •OH generation. The results confirm that surface hydroxyl groups have an interaction with ozone adsorption on catalyst surfaces. Pumice can adsorb ozone molecules in water, and the adsorbed ozone molecules can react with surface hydroxyl groups on metal oxides of pumice to generate •OH, which in turn oxidize *p*-CNB. Increasing Fe results in the enhancement of surface hydroxyl groups and an increase in the amount of ozone adsorption, as well as in the remarkable enhancement of the probability of reaction between ozone in water and surface hydroxyl groups on metal oxides that accelerate •OH generation from ozone decomposition and promote *p*-CNB removal.

4. Conclusions

The Fe/pumice, as an ozonation catalyst, significantly increases the removal efficiency of *p*-CNB, the utilization efficiency of ozone, and •OH production relative to pumice and is stable during catalytic ozonation. Fe-modified pumice increased BET surface area and surface hydroxyl concentration, and decreased the mass ratio of SiO_2 /metal oxide and the average pore diameter. The mesoporous structure is a key factor for ozone adsorption onto Fe/pumice. Surface hydroxyl groups on metal oxides of the Fe/pumice surface are also ozone decomposition sites. The uncharged surfaces hydroxyl groups benefited the catalytic activity of the Fe/pumice. The Fe/pumice catalyst has more ozone decomposition sites and higher ozone adsorption ability than pure pumice. This enhancement significantly increased •OH generation in the reaction systems. These changes remarkably enhance the removal efficiency of *p*-CNB at the heterogeneous interface and increase the rate of *p*-CNB oxidation reactions in aqueous solution.

Acknowledgments

The support from the National Natural Science Foundation of China (Grant No. 51208186), the China Post Doctoral Science Foundation (Grant No. 2015M570387), the Funds for Creative Research Groups of China (Grant No. 51121062), the State Key Laboratory of Urban Water Resource and Environment (Grant No. 2014TS03) and the Youth Foundation of Harbin (Grant No. 2014RFQYJ182) are greatly appreciated.

References

[1] T. Zhang, H.B. Zhu, Z.Q. He, J.P. Croue, Environ. Sci. Technol. 47 (2013) 2784–2791.
[2] S. Song, Z.W. Liu, Z.Q. He, A.L. Zhang, J.M. Chen, Environ. Sci. 44 (2010) 3913–3918.
[3] Z.Q. Liu, J. Ma, Y.H. Cui, L. Zhao, B.P. Zhang, Appl. Catal. B: Environ. 101 (2010) 74–80.
[4] M.H. Sui, S. Xing, L. Sheng, S. Huang, H. Guo, J. Hazard. Mater. 227 (2012) 227–236.
[5] L. Li, W.Y. Ye, Q.Y. Zhang, F.Q. Sun, P. Lu, X.K. Li, J. Hazard. Mater. 170 (2009) 411–416.
[6] J. Ma, N.J.D. Graham, Water Res. 33 (1999) 785–793.
[7] R. Rosal, A. Rodrgiuez, M.S. Gonzalo, E. Garcia-Calvo, Appl. Catal. B: Environ. 84 (2008) 48–57.
[8] Y. Dong, H.X. Yang, K. He, S.Q. Song, A.M. Zhang, Appl. Catal. B: Environ. 85 (2009) 155–161.
[9] B. Kasprzyk-Hordern, U. Raczyk-Stanisawiak, J.S. wietlik, J. Nawrocki, Appl. Catal. B: Environ. 62 (2006) 345–358.
[10] R. Andreozzi, M.S. Lo Casale, R. Marotta, G. Pinto, A. Pollio, Water Res. 34 (2000) 4419–4429.
[11] P.C.C. Faria, J.J.M. Orfao, M.F.R. Pereira, Appl. Catal. B: Environ. 88 (2009) 341–350.
[12] M. Muruganandham, J.J. Wu, Appl. Catal. B: Environ. 80 (2008) 32–41.
[13] F.J. Beltran, F.J. Rivas, R. Montero-de-Espinosa, Water Res. 39 (2005) 3553–3564.
[14] J. Zhang, K.-H. Lee, L. Cui, T.-S. Jeong, J. Ind. Eng. Chem. 15 (2009) 185–189.
[15] W. Qin, X. Li, J. Qi, Langmuir 25 (2009) 8001–8011.
[16] J. Ma, M.H. Sui, T. Zhang, C.Y. Guan, Water Res. 39 (2005) 779–786.
[17] R.C. Martins, R.M. Quinta-Ferreira, Appl. Catal. B: Environ. 90 (2009) 268–277.
[18] R. Gracia, S. Cortes, J. Sarasa, P. Ormad, J.L. Ovelleiro, Water Res. 34 (2000) 1525–1532.
[19] H.N. Li, B.B. Xu, F. Qi, D.Z. Sun, Z.L. Chen, Appl. Catal. B: Environ. 152–153 (2014) 342–351.
[20] L. Yuan, J.M. Shen, Z.L. Chen, Y. Liu, Appl. Catal. B: Environ. 117–118 (2012) 414–419.
[21] S.S. Kaplan Bekaroglu, N.O. Yigit, T. Karanfil, M. Kitis, J. Hazard. Mater. 183 (2010) 389–394.
[22] M. Yavuz, F. Gode, E. Pehlivan, S. Ozmert, Y.C. Sharma, Chem. Eng. J. 137 (2008) 453–461.
[23] K. Venkata Subba Rao, M. Subrahmanyam, P. Boule, Appl. Catal. B: Environ. 49 (2004) 239–249.
[24] K. Venkata Subba Rao, M. Subrahmanyam, P. Boule, Appl. Catal. B: Environ. 46 (2003) 77–85.
[25] J. Nawrockia, B. Kasprzyk-Hordern, Appl. Catal. B: Environ. 99 (2010) 27–42.
[26] T. Zhang, J. Ma, J. Mol. Catal. 279 (2007) 82–89.
[27] Z.Z. Xu, Z.L. Chen, C. Joll, Y. Ben, J.M. Shen, H. Tao, Catal. Commun. 10 (2009) 1221–1225.
[28] Y. Liu, J.M. Shen, Z.L. Chen, L. Yang, Y. Han, Appl. Catal. A: Gen. 403 (2011) 112–118.
[29] L. Yuan, J.M. Shen, Z.L. Chen, Water Sci. Technol. 68 (2013) 1895–1900.
[30] H. Bader, J. Hoigné, Water Res. 15 (1981) 449–456.
[31] H. Tamura, A. Tanaka, K.Y. Mita, R. Furuichi, J. Colloid Interface Sci. 209 (1999) 225–231.
[32] J.S. Noh, J.A. Schwarz, J. Colloid Interface Sci. 130 (1989) 157–164.
[33] G.L. Richmond, Chem. Rev. 102 (2002) 2693–2724.
[34] M. Zic, M. Ristic, S. Music, J. Alloys. Compd. 431 (2007) 54–56.
[35] S. Krehula, S. Music, J. Mol. Struct. 834–836 (2007) 154–161.
[36] J.M. Shen, Z.L. Chen, Z.Z. Xu, J. Hazard. Mater. 152 (2008) 1325–1331.
[37] B. Legube, V.L.N. Karpel, Catal. Today 53 (1999) 61–72.
[38] L. Zhao, J. Ma, Z.Z. Sun, H.L. Liu, Environ. Sci. Technol. 43 (2009) 2047–2053.
[39] W. Stumm, Chemistry of the Solid–Water Interface, John Wiley & Sons, New York, 1992, pp. 15–20.
[40] W. Stumm, J.J. Morgan, Aquatic Chemistry: Chemical Equilibria and Rates in Natural Waters, John Wiley & Sons, New York, 1996, pp. 533–541.
[41] M.H. Sui, L. Sheng, K.X. Lu, F. Tian, Appl. Catal. B: Environ. 96 (2010) 94–100.

[42] L. Yang, C. Hu, Y.L. Nie, J.H. Qu, Appl. Catal. B: Environ. 97 (2010) 340–346.
[43] T. Zhang, C.J. Li, J. Ma, H. Tian, Z.M. Qiang, Appl. Catal. B: Environ. 82 (2008) 131–137.
[44] W.J. Masschelein, Unit Processes in Drinking Water Treatment, Marcel Dekker, New York, 1992, pp. 67–122.
[45] T. Zhang, W.W. Li, J.P. Croue, Environ. Sci. Technol. 45 (2011) 9339–9346.
[46] H. Fujita, J. Izumi, M. Sagehashi, T. Fujii, A. Sakoda, Water Res. 38 (2004) 159–165.
[47] B. Kasprzyk-Hordern, M. Ziólek, J. Nawrocki, Appl. Catal. B: Environ. 46 (2003) 639–669.